Detection and sizing of disbond in multilayer bonded structure using modally selective guided wave

Kai WANG[a], Menglong LIU[b*], Wuxiong CAO[a], Weidong YANG[c], Zhongqing SU[a,d], Fangsen CUI[b]

[a] Department of Mechanical Engineering, The Hong Kong Polytechnic University, Hong Kong SAR

[b] Institute of High Performance Computing, A*STAR, Singapore 138632, Singapore

[c] Department of Materials Science and Engineering, National University of Singapore, 117583, Singapore

[d] The Hong Kong Polytechnic University Shenzhen Research Institute, Shenzhen 518057, P.R. China

Submitted to *Structural Health Monitoring - An International Journal*

(initial submission on 29 March 2019, revised and re-submitted on 23 June 2019)

[*] To whom correspondence should be addressed. Tel.: +65-64191130, Email: liumenglong1988@gmail.com (Dr. M. LIU)

Abstract

Bonded structures are frequently adopted in structural connections and are highly prone to degradation or decrease of interfacial strength due to adhesive aging, poor quality of surface preparation, as well as the exposure to harsh environment and external loading. This study addresses the establishment of a framework, in which a modally selective ultrasonic guided wave (UGW) is used for disbond identification and sizing. In this framework, the propagating and evanescent modes of UGWs are first obtained, followed by the excitability analysis for each UGW propagating mode, providing a theoretical basis for effective wave excitation in the experiment. Then the interaction of UGW with disbond is interrogated analytically using a method combining semi-analytical finite element (SAFE) and normal mode expansion (NME), whereby wave transmission, wave reflection, and mode conversion can be calculated quantitatively. Taking all these aspects into account, mode 11 at around 3.85 MHz features a high propagation velocity, large mode excitability, and increasing amplitude drop with the enlargement of disbond size, and is thus selected for disbond detection. Both numerical and experimental validations are performed, in which disbonds of different lengths from 10 mm to 40 mm are examined, and the results well corroborate the effectiveness of the proposed framework for UGW-based disbond detection.

Keywords: Adhesive bonded joint; semi-analytical finite element; normal mode expansion; disbond detection; guided wave

1. Introduction

Adhesively bonded joints are one of the most frequently adopted connections in engineering structures [1,2]. Suffering from various harsh environmental invasions, external loading, and natural aging, the quality of adhesive bonding may be degraded, resulting in disbond or decrease of the interfacial strength of the bonded joints [3,4]. A timely and accurate assessment of bonding quality is crucial to structure integrity, to fulfill which numerous methods have been investigated [5–12]. Among these methods, non-destructive evaluation (NDE) methods based on ultrasonic bulk wave are now prevalently adopted in industries [12]. Nevertheless, in these methods, the inspection is performed in a point-to-point fashion, which is time consuming and labor intensive, and may not be effective to access hidden regions.

To overcome this deficiency, ultrasonic guided waves (UGWs), propagating along the in-plane direction of layer joint structure composed of adherend and adhesive layer, offer an alternative approach to evaluate the health condition of the adhesive bonded structure. Compared with conventional bulk wave-based NDE, the advantages of the guided wave-based technique [13–16] include the capability to inspect a large range, accessibility to hidden structures, and *in situ* and real time monitoring of structural health status. Representatively, Yuan and Qiu et al designed a creative multi-response wireless monitoring network [13], proposed a promising guided wave-based Gaussian mixture model [14], and a time reversal-based structural imaging methods [15], via which the damage and impact of complex aircraft composite structure are successfully monitored. This guided wave-based technique enables a line-to-line inspection, which improves the efficiency of damage detection significantly.

The effectiveness of the UGW-based methods lies in a premise that the propagation of UGW is disturbed by the disbond, leading to wave reflection, wave transmission, or mode conversion,

and thus disbond can be characterized making use of the disbond-related features endowed in the UGWs. On this basis, numerous works have been performed [17–19], in which UGWs of specific mode-frequency combination, with large in-plane displacement at the adhesive layer [17] or large in-plane shear stress at the adhesive-adherend interface [18], have been adopted. Using the above selected UGW modes, disbond in the bonded structures is detected, albeit at a qualitative level targeting a specific structure. Nevertheless, when extended to quantitative characterization of the disbond defect, existing disbond detection ideas using UGW modes are confronted with bottlenecks, since there is rarely a comprehensive interpretation for the modulation mechanism of the disbond on UGW propagation.

Different from defects which induce energy scattering or reflection (e.g. fatigue cracks), the disbond defect is parallel to the UGW propagation direction, and thus it modulates UGW via a different mechanism. As pointed out by Cawley et al. [20], the property of UGW is principally determined by the adhrend layer, attributed to the marginal thickness and stiffness of adhesive layer compared with those of the adhrend layer. Herein energy of the incident UGW is almost entirely transmitted when traversing a disbond, leading to energy transfer from one incident mode to multiple modes. This energy transfer linked with mode conversions accounts for the disbond-related feature changes in the UGW signals, and by analyzing the mode conversions, the disbond can be evaluated. Fromme et al. [21] discovered a dominant UGW transmission, together with a minor UGW reflection from the disbond tip, but that reflection signal may be prone to be contamination from noises. Ren and Lissenden [22] recently applied two-dimensional frequency domain finite element method to analyze UGW interaction with disbond in composite adhesive joint, but a sophisticated handling of modeling details and a large computation effort in COMSOL are required. Several other analytical and numerical ideas are also approached, for example, Wiener-Hopf technique [23], analysis of dispersion curve obtained

from global matrix method [24], time-domain finite element analysis (FEA) [25], and normal mode expansion (NME) [26]. But these works focus on the influence of bonding quality on UGW propagation in single lap joints, instead of UGW interaction with disbond in multilayer bonded structures. In sum, there still entails the development of an efficient and effective approach to correctly understand UGW interaction with disbond in multilayer bonded structures.

In addition to the interpretation for modulation mechanism of disbond on UGW propagation, it is also demonstrated in previous researches [20,27,28] that the excitability/sensibility of selected UGW with a specific mode-frequency combination is of practical significance. For example, a 'true' guided wave by adhesive layer, in which the energy is mostly confined within the adhesive layer, is sensitive to disbond [29], but suffers a poor excitability from the surface of adhrend by UGW actuator. Thus the termed 'true' guided wave is far from a practical application to disbond detection. To selectively excite a specific UGW, several excitation methods were previously attempted. Piezoelectric wafer active sensors mounted on the surface are able to fulfill a mode tuning of fundamental A_0 and S_0 mode, while fail to tune higher modes [30]. Comb shape-based transducer array is proposed [31], with higher mode modulation capability testified. Following the similar principle, longitudinal wave transducer mounted on the angle beam wedge [28] is another approach for mode tuning. By tuning the wedge angle, UGW with desired phase velocity range can be preferably excited. Despite that, as multiple UGW modes are often covered in the preferred frequency range, a quantitative analysis of mode excitability is still to be developed.

To overcome the deficiencies aforementioned, it is an imminent task to develop a universal approach for the UGW-based disbond detection, which is capable of identifying and quantifying disbond defects. As stated earlier, this approach entails research efforts on the investigation of

mechanism of UGW interaction with disbond and the excitability/sensibility of UGW. On top of these two aspects, to further warrant the applicability of UGW-based method, another supplementary point, as stressed in almost all the UGW-based defect detection, is that the selected UGW should be easily separated from other possibly excited modes. Particularly, as the increase of incident frequency, the selected UGW may be submerged in multiple modes that are simultaneously excited. All the three points, if well addressed, can facilitate the development and deployment of UGW-based approach for disbond detection.

Addressing the above concerns, in this study, a framework is constructed towards a UGW-based approach, which, by making use of modally selective UGW, is capable of identifying and quantitatively sizing disbond. In this approach, a hybrid model combining semi-analytical finite element (SAFE) and normal mode expansion (NME) is developed to quantitatively analyze the interaction of UGW with disbond of different sizes. This hybrid model features a process to quantitatively obtain each UGW mode in transmitted and possibly reflected wavefields when UGW encounters a disbond. In addition, excitability of UGW under each mode-frequency combination is scrutinized based on the mode shape and power flux. At last, to facilitate the separation of selected UGW mode from other excited modes, the group velocity is examined to warrant that the interested UGW mode arrives at the sensor earlier than other modes. Using this framework, the UGW-based technology for disbond detection in a bonded structure with arbitrary cross section can be deployed and implemented in practice.

This paper is organized as follows. Section 2 introduces the analytical framework for mode selection, followed by the numerical and experimental validation of disbond detection of different sizes in Section 3. Concluding remarks are drawn in Section 4.

2. Analytical framework for mode selection

2.1 Problem statement

As illustrated in Figure 1, a disbond defect exists in a three layer Al-epoxy-Al bonded structure. The UGW is excited from the incidence region, and upon traversing the disbond defect region, it is transmitted to the transmission region. In the disbond region, considering that the disbond disconnects the top Al adherend from the adhesive layer, the incident UGWs are converted into waves propagating independently on the top Al adherend layer and the bottom Al-epoxy bonded layer. Two interfaces (denoted by Interface I and Interface II) are defined to represent the site at which UGW enters and exits the disbond region. To improve the sensitivity and to enhance the reliability of the UGW-based disbond detection, several key points should be addressed from both theoretical and practical perspectives. Theoretically, together with the phase and group velocities, interpretation of the mechanism behind the interaction of UGW with disbond provides a basis for the selection of preferred UGW and extraction of signal feature for disbond detection. Practically, as multiple UGW modes co-exist in the structure, excitation and acquisition of UGW in which the preferably selected mode dominates are critical for the quantitative evaluation of disbond. To address a step-to-step solution to all these issues, a framework is proposed, as illustrated in the flowchart in Figure 2. Via the proposed framework, the UGW modes with the potential for quantifying the disbond in practical application are selected, which should satisfy the following criteria: (1) appropriate group velocity, enabling isolation of preferred wave packet from other excited UGW modes; (2) high sensitivity to disbond defect; and (3) large excitability. Each key step in the flowchart and each criteria are elaborated in the following section.

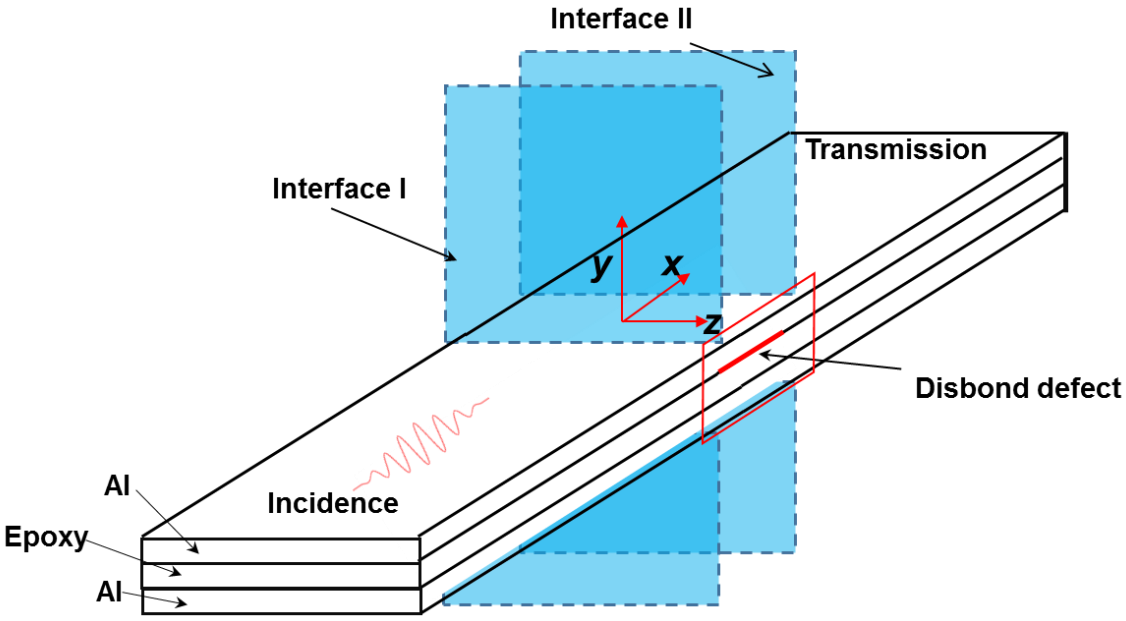

Figure 1 Illustration of UGW-based disbond detection (epoxy layer thickness is artificially enlarged to improve its visibility).

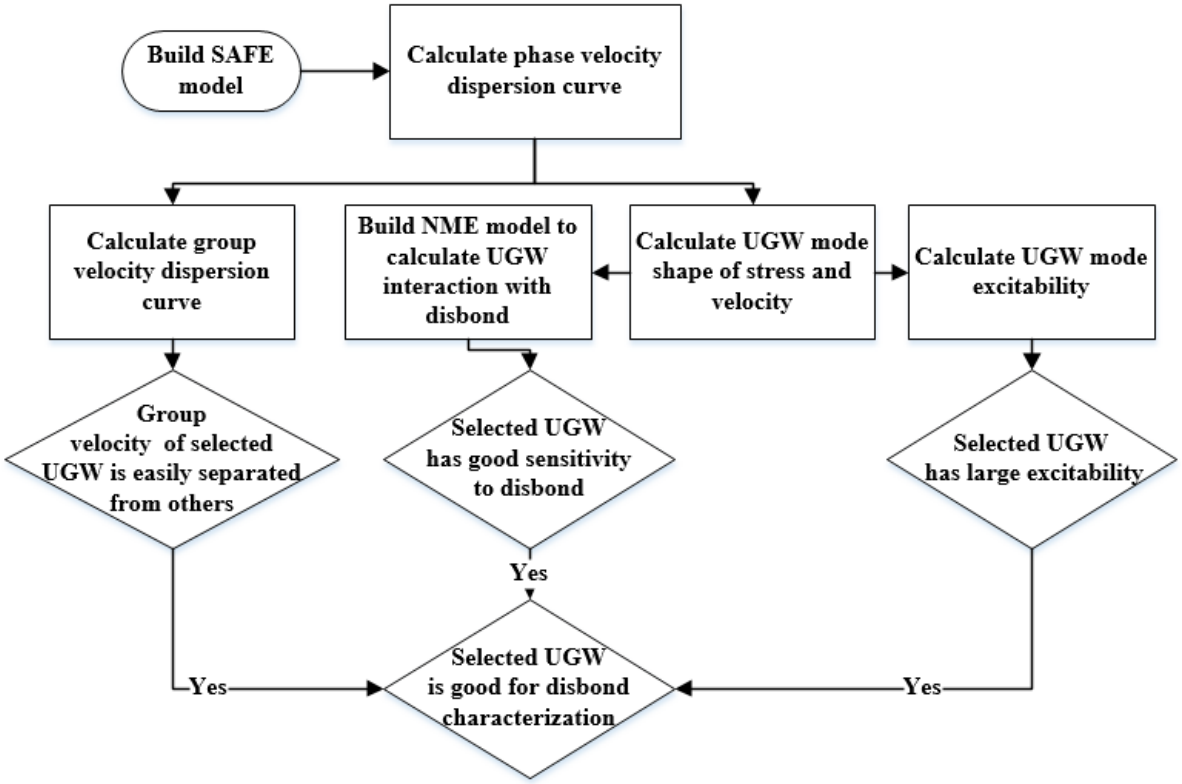

Figure 2 Analytical framework for mode selection for disbond detection.

2.2 Dispersion curves

When a plane crested wave is incident from the bonded region, the multilayer structure can be deemed as a two-dimensional waveguide, which can be delineated using a plane strain model. One-dimensional SAFE [32,33] is adopted to calculate the dispersion curves of phase and group velocity of propagating modes in Al-epoxy-Al, Al-epoxy, and Al structures (see Figure 3). SAFE offers a powerful numerical method to obtain dispersion curves and mode shapes of UGW in cross section of arbitrary shape. The material parameters are listed in Table 1. Al 6061 and Hysol® PL7000 are adopted as the adhrend and adhesive layers respectively. From the phase velocity dispersion curve displayed in Figure 3a and b, it is clear that: (1) curves for Al-epoxy, Al, and Al-epoxy-Al are largely quasi-overlapped, because the propagation characteristics of UGW mainly rely on the adhrend, and hence slight uncertainty in the epoxy property is of minor influence on UGW [20], and (2) in a few regions, the curves are separated (e.g. modes 1 and 2 over 3.5 MHz), and the UGWs in these region are termed 'true' guided waves since the energy is constrained mainly within the adhesive layer. In these regions, epoxy property should exert a decisive influence on UGW propagation.

In the proposed framework, group velocity (see Figure 3c and d) is a significant aspect when a selected higher mode is excited together with other multiple possibly co-excited modes. To make the interested mode dominantly acquired and easily discernable over other modes, two requirements should be satisfied, (1) a higher and stable group velocity in the excited finite frequency band and (2) the UGW with specific mode-frequency combination should be well separated from other possibly excited UGW modes in the time domain. Besides the dispersion curve, the wave structure can also be obtained via SAFE, and this provides the theoretical basis for the investigation of mode excitability and analysis of interaction between incident UGW and disbond.

Table 1 Material parameter of aluminum and epoxy.

Part	Elastic modulus (GPa)	Poisson's ratio	Density (kg/m^3)
Aluminum 6061	68.9	0.33	2780
Epoxy	1.8	0.402	1104

(a)

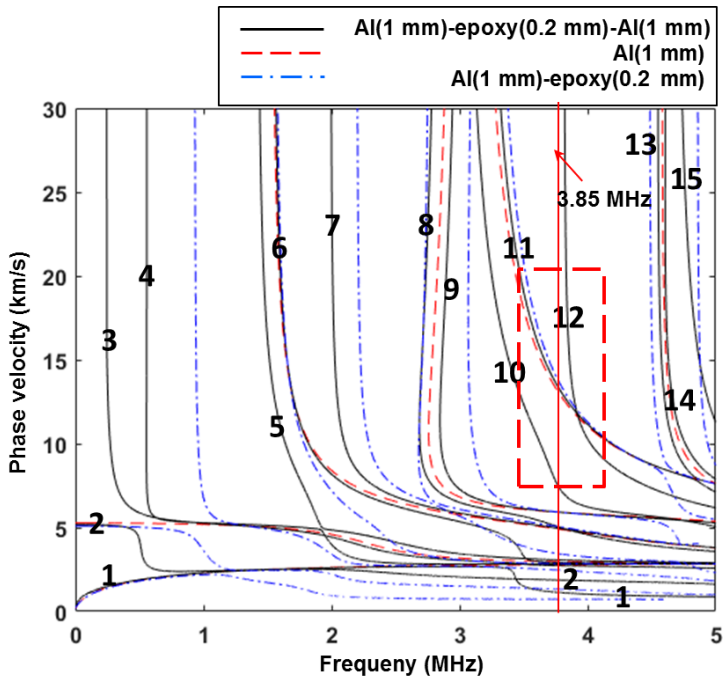

(b)

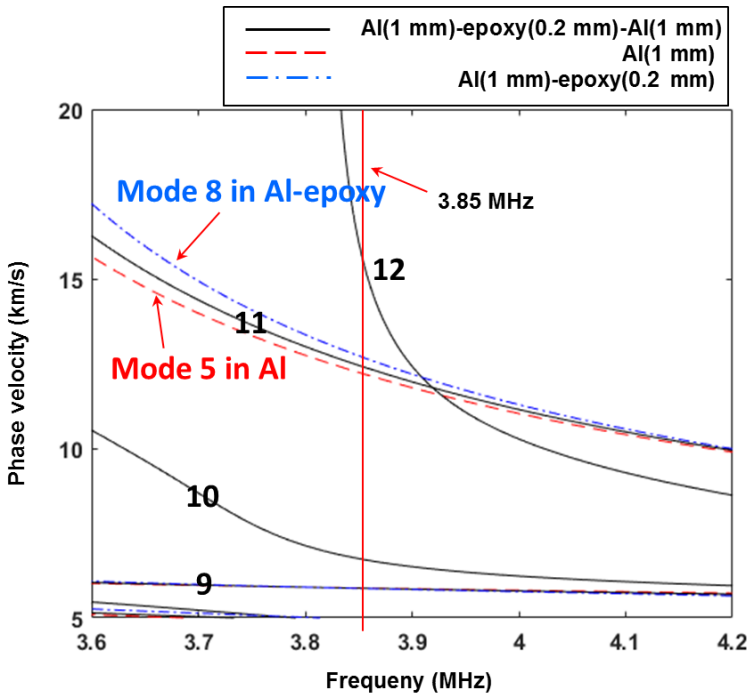

(c)

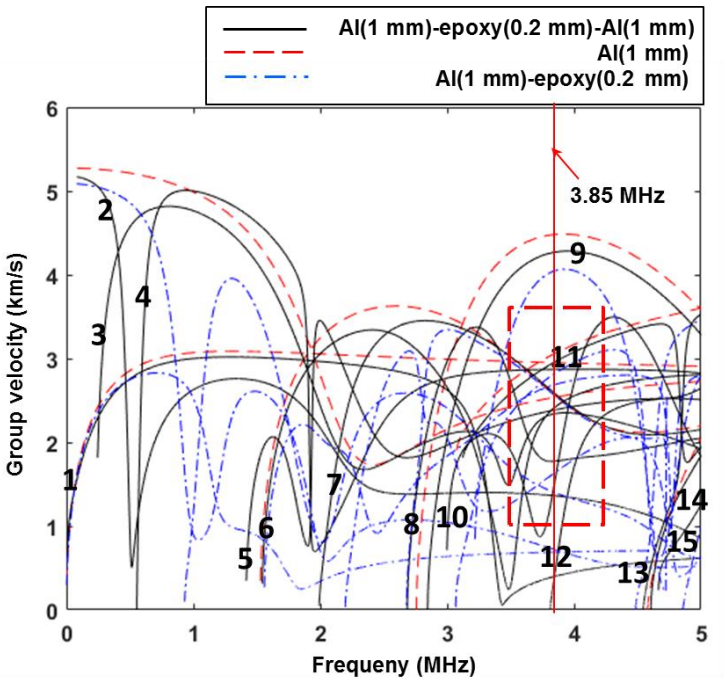

(d)

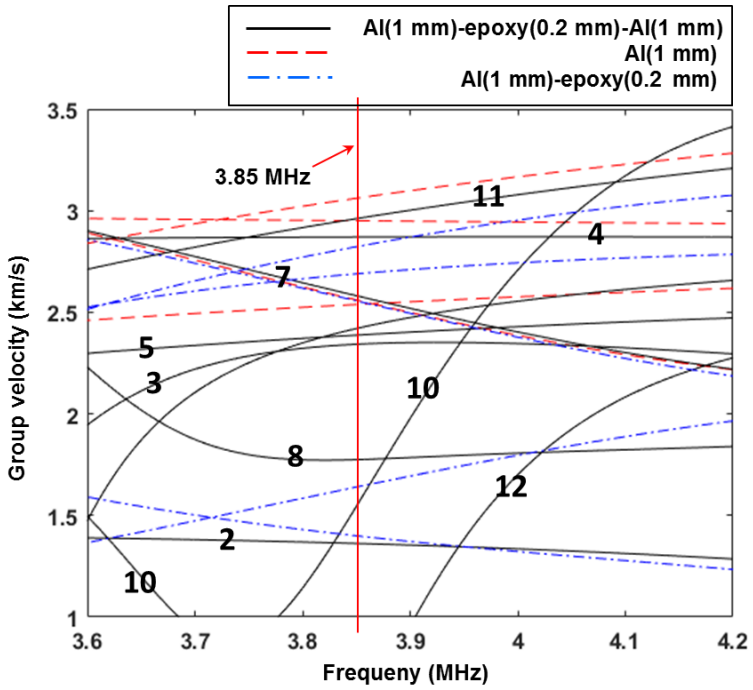

Figure 3 Phase velocity and group velocity dispersion curve of UGW (a) phase velocity, (b) zoom-in of phase velocity, (c) group velocity, and (d) zoom-in of group velocity. (only UGWs in Al-epoxy-Al are indexed).

2.3 Mode excitability and sensibility

To facilitate the practical implementation of the proposed UGW-based approach, it is required

that the selected UGW features a higher excitability and sensibility than the rest of wave modes that could be possibly excited, and this guarantees that the selected UGW is preferably excited/sensed. In this study, the excitation is generated using a piezoelectric transducer, and then via the angle beam wedge, it is transmitted to the adherend surface of the bonded structure. An inviscid couplant is used in the experiment to couple the loading from angle beam wedge to the inspected bonded structure, and thus only the out-of-plane loading is applied normal to the adherend surface. A quantitative description of the mode excitability, given the out-of-plane loading, is derived as [34]

$$\mathbf{v}(x,y)=\sum_{n} a_n(x)\mathbf{v}_n(y) \propto \sum_{n} \frac{v_{y,n}(y)}{P_{nn}}\mathbf{v}_n(y) \quad , \tag{1}$$

where $\mathbf{v}(x,y)$ is the velocity vector superposed from all the n possibly excited UGW modes, $v_{y,n}(y)$ is the component of velocity vector in the out-of-plane loading direction for mode n. $a_n(x)$ is the amplitude of mode n, $\mathbf{v}_n(y)$ is the velocity vector corresponding to the power flux P_{nn} along x direction. Provided a normalized power flux P_{nn}, the calculated value of $v_{y,n}(y)$, a representation of mode excitability, is displayed in Figure 4. Note that although in some numerical simulations the 'true' guided wave (mode 1 and 2 over 3.5 MHz) is proven to be sensitive to disbond [29], it is hard to be excited from the adherend surface in the experiment, since its excitability approaches zero. Besides that, at the cut-off frequency of several modes, e.g. modes 4, 8, 9, 14, and 15, a large excitability is obtained. Nevertheless, the corresponding group velocities approach zero (see Figure 3c), and thus the wave packets are elongated and distorted in the time domain, and lag behind other excited modes in the time domain, all of which perplex the signal acquisition and interpretation. Hence, the UGW with moderately large excitability yet minute group velocity dispersive properties, e.g. mode 11 in the frequency range from 3.5 MHz to 4 MHz, bears higher potential of practical application. With the excitability of each mode, candidates with practical application potential can be selected, and in order to

utilize the selected UGW mode for quantitative sizing of disbond, the modulation mechanism of disbond on the UGW is to be investigated.

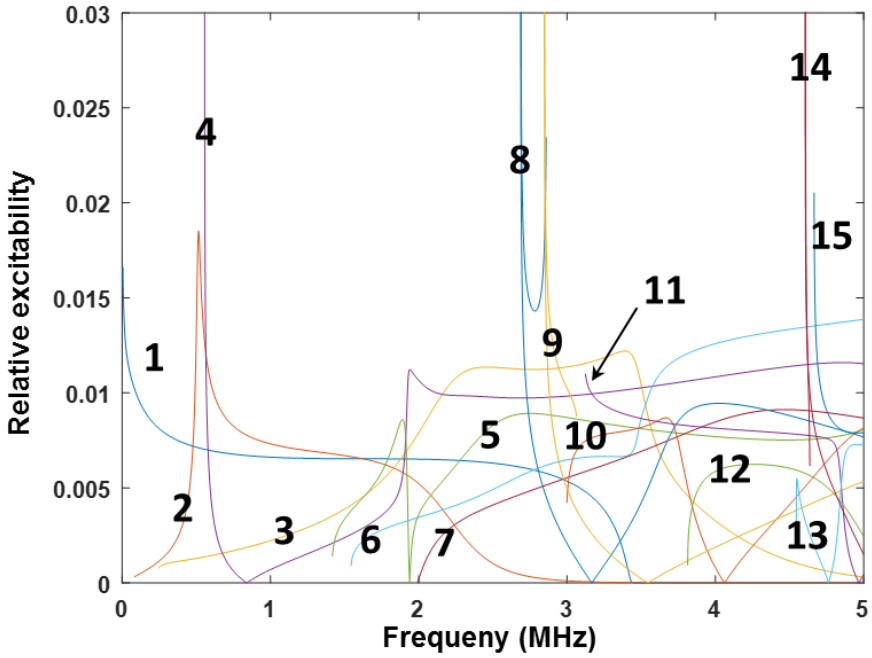

Figure 4 Mode excitability in the bonded structure with out-of-plane loading.

2.4 Wave interaction with disbond

Considering that the disbond introduces a separation between the adhesive and adherend, the UGW interaction with disbond, in essence, entails the scrutinization of the wave scattering and mode conversion at (1) Interface I, where the incident UGW propagates from bonded structure to the disbond region composed of separated Al and Al-epoxy structure, and (2) Interface II, where the UGW is transmitted to bonded structure (see Figure 1a). To this end, a hybrid approach combining SAFE and NME is developed here.

A typical dispersion curve calculated via SAFE, including both propagating mode and evanescent mode, is displayed in Figure 5, where w, h, c_T, and k denote angular frequency, plate thickness, shear wave velocity, and wave number, respectively. The "purely real k" denotes the propagating mode, while "purely imag k" and "complex k" are both evanescent

modes that attenuate rapidly along the propagation direction. Then the calculated displacement and stress fields of both propagating and evanescent modes by SAFE are input to NME model to analyze the wave propagation with disbond.

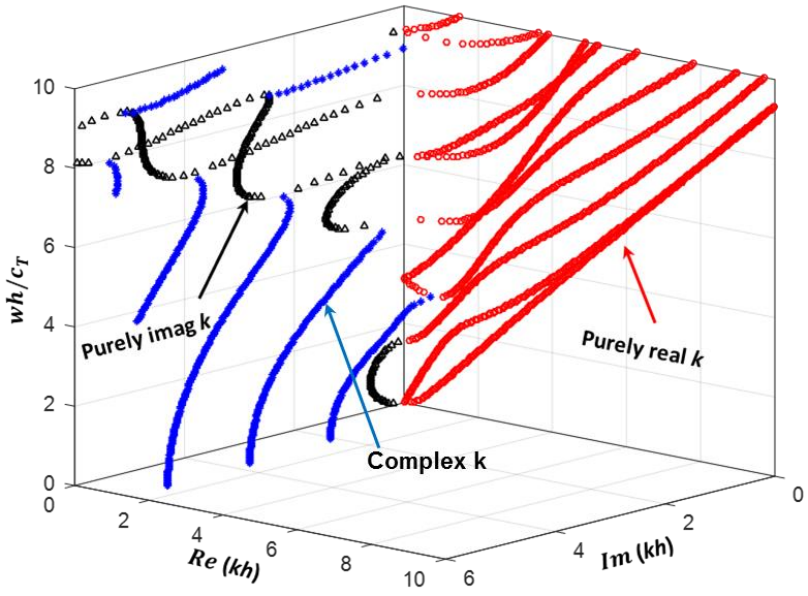

Figure 5 Dispersion relation including both propagating and evanescent modes.

Take the structure in Figure 1 for the illustration of NME (see Figure 6). Song et al. [26] and Puthillath et al. [35] gave a detailed mathematical description of NME. To utilize NME for the investigation of disbond effect on UGW propagation, several major improvements are made in this study towards the previously developed NME. In the previous NME model, only the interaction of UGW with plate overlap without adhesive layer [26] and with single-side lap joint [35] is investigated. In this study, a quantitative calculation of energy transmission and reflection of each mode through both interfaces of disbonds is developed. When one UGW mode with a specific frequency is incident into the bonded structure, the interaction of UGW with disbond at Interface I can be depicted based on enforced stress and displacement continuities at both sides of Interface I, whereby the amplitude of each transmitted UGW mode in the disbond region, as well as the reflected UGW mode back to the incidence bonded region, can be calculated. The transmitted UGWs further propagate separately along Al and Al-epoxy layers,

before arriving at Interface II. Following the same calculation procedure at Interface I, the transmitted energy to the transmission bonded region via Interface II can also be calculated. In these calculations, quadratic elements are assigned at both interfaces, and stress and displacement continuities are satisfied on all the Gaussian integration points of elements.

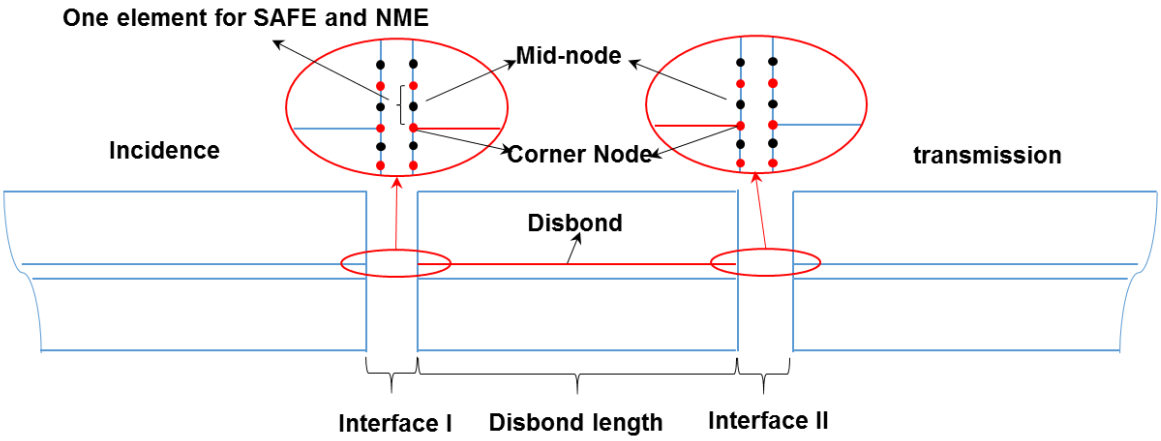

Figure 6 Illustration of NME model based on stress and displacement continuity at two interfaces.

As explained in Section 2.3, the UGW mode 11 turns out to be a potential candidate for disbond detection, attributed to moderately large excitability yet minute group velocity dispersive properties, and hence it is adopted here for illustration of the modulation of disbond on UGW. As the phase velocity of mode 11 from 3.5 MHz to 4 MHz in the bonded structure is close to that of mode 5 in single Al layer and mode 8 in Al-epoxy layer (see two curves at Figure 3b around mode 11 at Al-epoxy-Al layer), the incident energy flux, expressed with Poynting vector, is almost evenly distributed to the two layers while traversing Interface I (see Figure 7a and b). Nevertheless, after propagation in the disbond region, UGW may not fully convert back to mode 11 in the transmission bonded region (see Figure 7c-e), and a portion of energy is finally transmitted to modes 10 and 12. At different disbond lengths, the transmitted energy of each UGW mode is different. This is attributable to that although mode 11 transmits to mode 5 in

the single Al layer and mode 8 in the Al-epoxy layer at Interface I, these two modes propagate at slightly different phase velocities, and thus after traversing disbond of different sizes, the constructed displacement and stress fields at Interface II are different from those at Interface I, leading to different energy transmission and mode conversion.

Via the proposed framework, the UGW mode with the potential for quantifying the disbond in practical application can be selected. As analyzed above, mode 11 in the frequency range from 3.5 MHz to 4 MHz (a corresponding wavelength around 3 mm) features a high excitability and sensibility, and the relation between the change in its amplitude of the transmitted energy and the length of disbond is explicitly ascertained. In addition, through the tuning of wedge angle, the selected mode 11 can be preferably excited, and has a higher group velocity than neighboring barely excited modes 10 and 12, both of which benefit the isolation and precise measurement of its magnitude. Accommodating all the concerns addressed in the introduction, mode 11 in the frequency range from 3.5 MHz to 4 MHz offers a desirable selection for the UGW-based disbond detection, which enables the disbond evaluation in a quantitative manner.

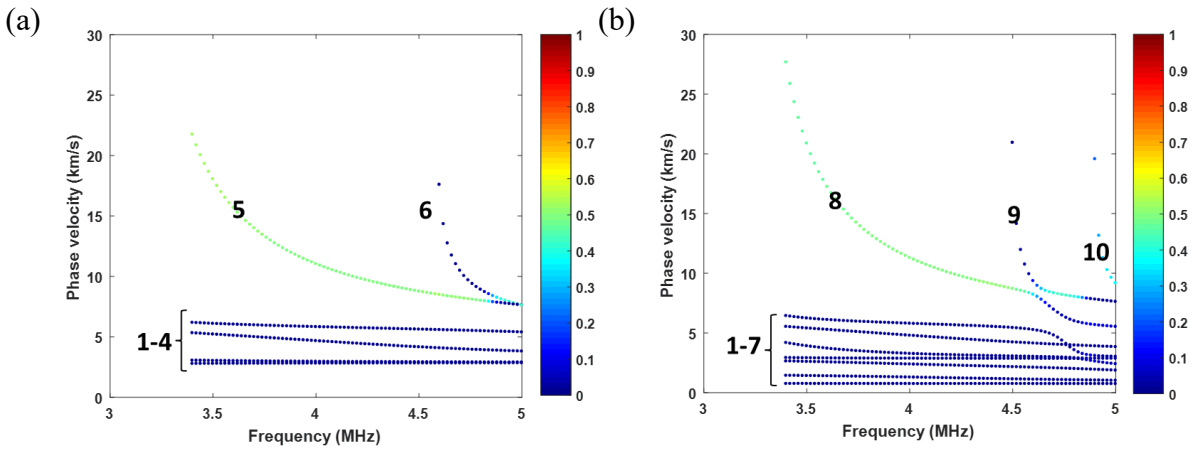

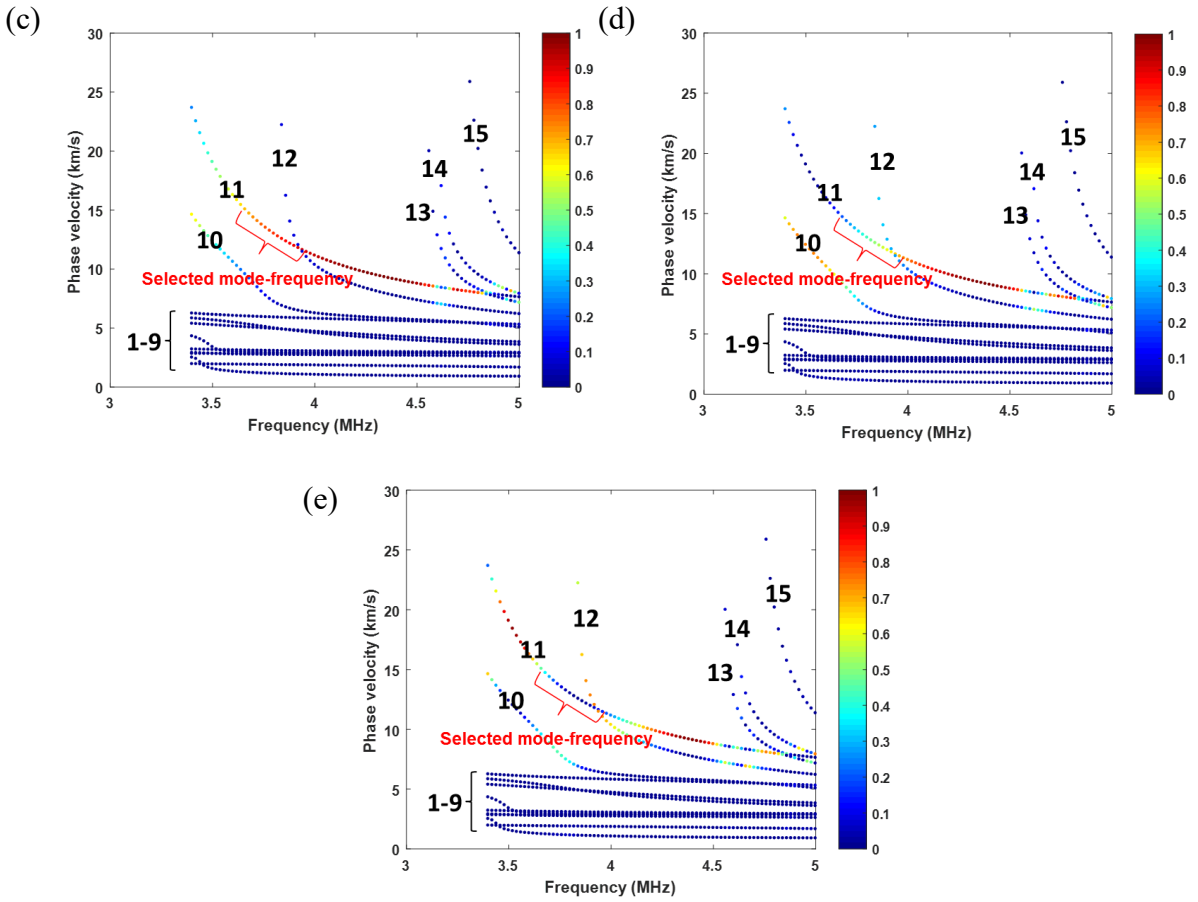

Figure 7 Energy distribution when the incident mode 11 interacts with disbond (a) energy transmission to single Al layer, (b) energy transmission to Al-epoxy layer, (c)-(e) energy transmission to bonded region with disbond length 10 mm, 20 mm, and 40 mm.

3. Numerical and experimental study

3.1 Experimental setup

For proof-of-concept, a multi-layer bonded structure is prepared in which two 300 mm × 300 mm Al-6061 plates measuring 1 mm in thickness are bonded using an epoxy film (Hysol® PL7000) with a uniform thickness of 0.2 mm. In this structure, artificial near zero-volume disbonds are introduced by placing Teflon inserts between one Al plate and the epoxy sheet adhesive, forming unbonded surfaces. Considering that the thickness of the Teflon film is 10 um, two disbonded surfaces separated by a thin layer form a zero-volume disbond defect. To avoid the generation of remarkable separation or void, the vacuum bagging is performed to

extract the air and to warrant the bonding quality. A schematic of the specimen and the defects is shown in Figure 8a, in which sizes of three disbond defects are 10 mm × 10 mm, 20 mm × 20 mm and 40 mm × 40 mm for D1, D2, and D3, respectively.

In the tests, a ten-cycle Hanning-window modulated sinusoidal tone burst is generated using a computer controlled system (Ritec® 5000 SNAP) to excite the probing waves. As shown in Figure 8b, two piston piezoelectric transducers (25.4 mm × 12.7 mm) with central frequencies of 5 MHz (as actuator and receiver, respectively) are coupled with the specimen via flexible angle beam wedges (FABW) (Panametrics® ABWX-2001). Wave signals acquired from 256 ultrasonic tests are averaged. A couplant (Olympus® Glycerin) is applied to ensure a consistent coupling between the transducer and FABW, as well as between FABW and the bonded structure. In the scanning process, 50 paths are defined, with some paths traversing the disbonded regions, while most paths traversing intact regions. The separation distance between two consecutive scanning paths is 10 mm.

In all the UGW tests, mode 11 at a central frequency 3.85 MHz is selected for further numerical and experimental validation. The skew angle between FABW and the bonded structure is set according to the Snell's law, calculated as $\arcsin(2.73/12.4) \approx 12.7^0$, where 2.73 km/s is the longitudinal wave velocity in FABW, and 12.4 km/s is the phase velocity of UGW mode 11 at 3.85 MHz, which gives a corresponding wavelength around 3.22 mm. Although mode 9 at around 3.85 MHz has higher group velocity than mode 11 (see Figure 3c and d), it is largely suppressed by both the angle setup and the corresponding poor excitability. Modes 10 and 12 may be excited, but with a much lower group velocity. Hence considering the aspects displayed in Figure 2 regarding mode excitability (see Figure 4), an appropriate sensitivity to disbond (see Figure 7c-e), and a high group velocity to be differentiated from other modes (2.96 km/s in

Figure 3d), mode 11 around 3.85 MHz forms a good candidate for disbond detection.

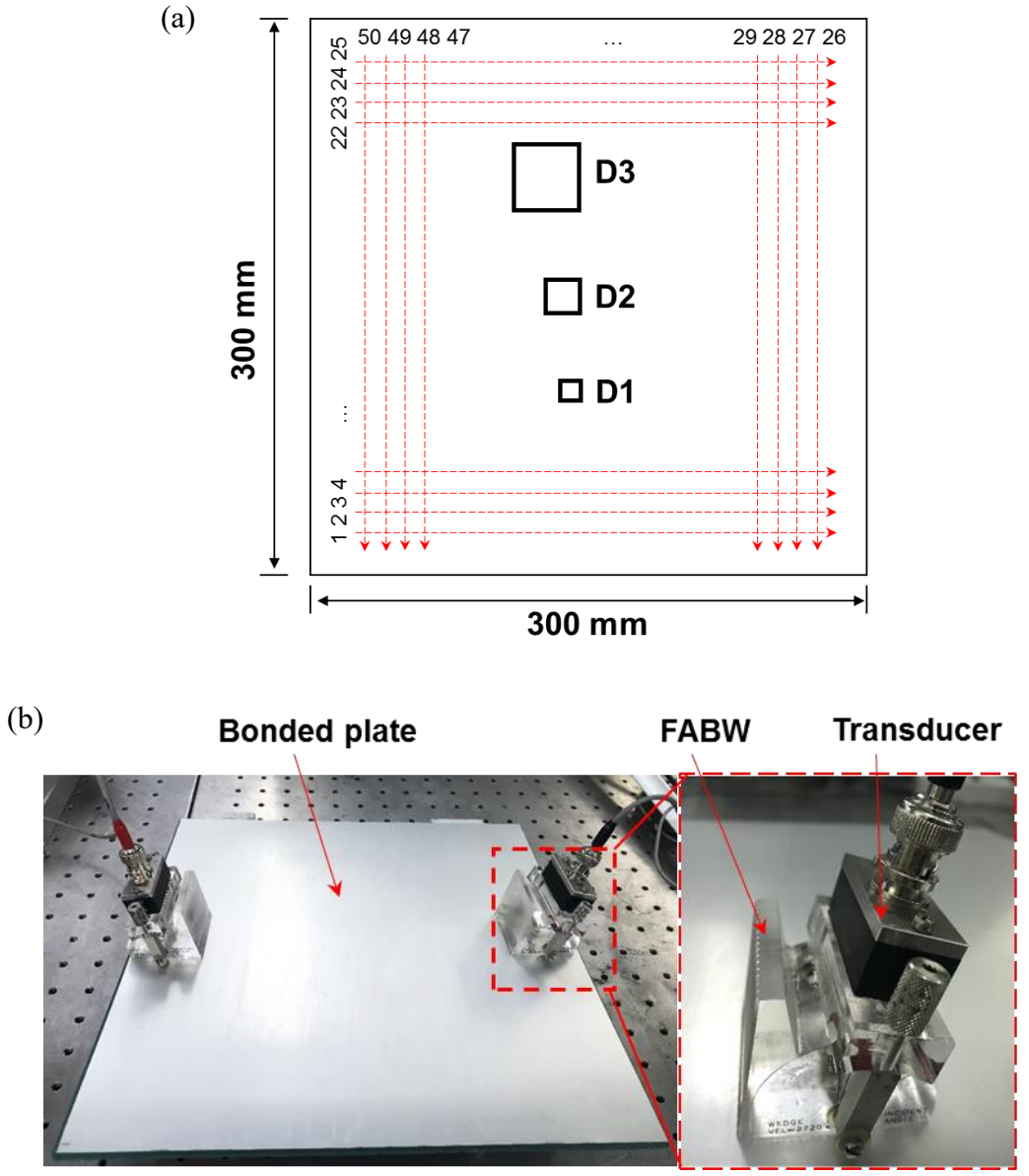

Figure 8 (a) Illustration of 50 scanning paths and three disbonds 10 mm × 10 mm, 20 mm × 20 mm, and 40 mm × 40 mm and (b) photograph of experiment.

3.2 Finite element model setup

A time domain finite element analysis (FEA) is performed with ABAQUS®, with the same setup as the experiment, as illustrated in Figure 9. A plane strain model is built, in which disbond is modeled with a seam between adhesive and adhrend layers. The linear element CPE4R is adopted throughout the model. A global mesh of 0.1 mm size is set, while a localized fine mesh

of 0.033 mm in the thickness direction is assigned to adhesive layer. In FEA model, the excitation generated by the transducer and through FABW to the bonded structure are modeled with an array of out-of-plane force, covering an entire loading length of 12.6 mm, and the phase of the force at individual points is delayed according to the angle of the wedge. The time delay between two neighboring excitation points is

$$\Delta t = \frac{\Delta s \times \sin(\alpha)}{v_{FAW}} = \frac{0.2\times10^{-3}\times\sin(12.7^0)}{2730} \approx 1.6106\times10^{-8} s\,, \tag{2}$$

where Δs, α, and v_{FAW} denote the distance between two neighboring excitation points, skew angle of FABW, and longitudinal wave velocity in FABW, respectively.

In a similar manner to wave excitation, the acquired wave signals via the transducer and FABW, which is tuned to preferably acquire UGW mode 11 at 3.85 MHz, is calculated using the delay and sum of the out-of-plane displacement at the sensing points with an interval of 0.1 mm, covering an entire sensing length of 12.6 mm. The superposed signal is obtained as

$$u_{add} = \sum_{i=1}^{i=126} u_i(t+(i-1)\Delta t_s)\,, \tag{3}$$

where 126 is the total number of sensing points, u_i is the out-of-plane displacement component for the i^{th} sensing point, and Δt_s denotes the time delay between two neighboring sensing points, which is 0.8053×10^{-8} s.

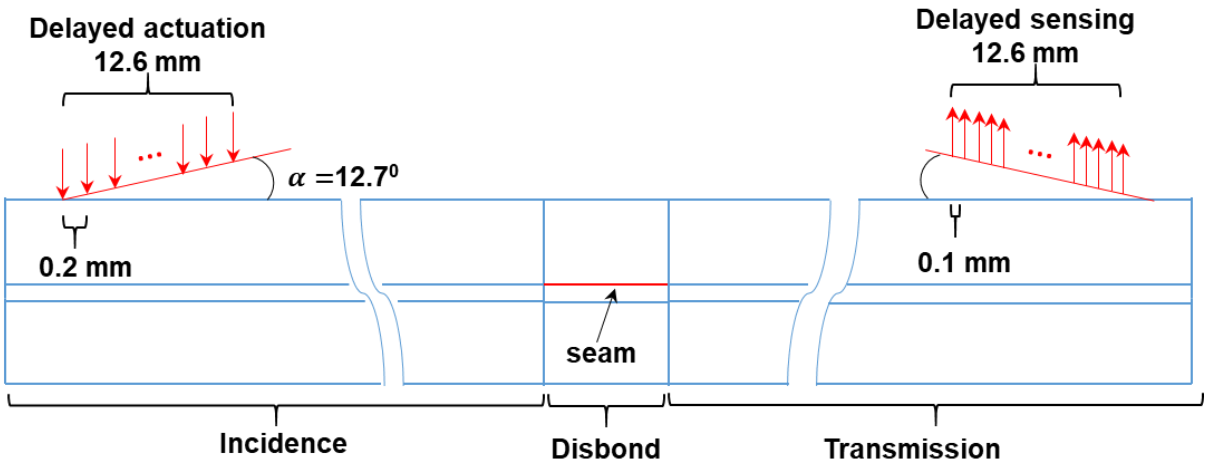

Figure 9 Illustration of FEA model with UGW propagating in bonded/disbonded structure.

3.3 Results and discussion

To analyze the excited UGW mode incident into the bonded structure, the two-dimensional fast Fourier transform is performed on the raw out-of-plane displacement signals at all the sensing points in the FEA model, to convert the energy distribution from the time-space domains to frequency-wave number domains. Via mathematical manipulations, the wave number domain is further converted to phase velocity domain, and then the ascertained energy spectrogram in the frequency-phase velocity domain is compared with the phase velocity dispersion curve, as displayed in Figure 10. The numerical model built with linear element shows some slight error in terms of phase velocity compared with theoretical curve, attributed to that ABAQUS®/Explicit only offers a linear element instead of higher order element for calculation. Still, it is clear that the spectrogram is dominated by mode 11 between 3.5 MHz and 4 MHz, owing to both large mode excitability (see Figure 4) of mode 11 and setup of skew angle, and accompanying the dominating mode 11, modes 10 and 12 of minor energy are also excited.

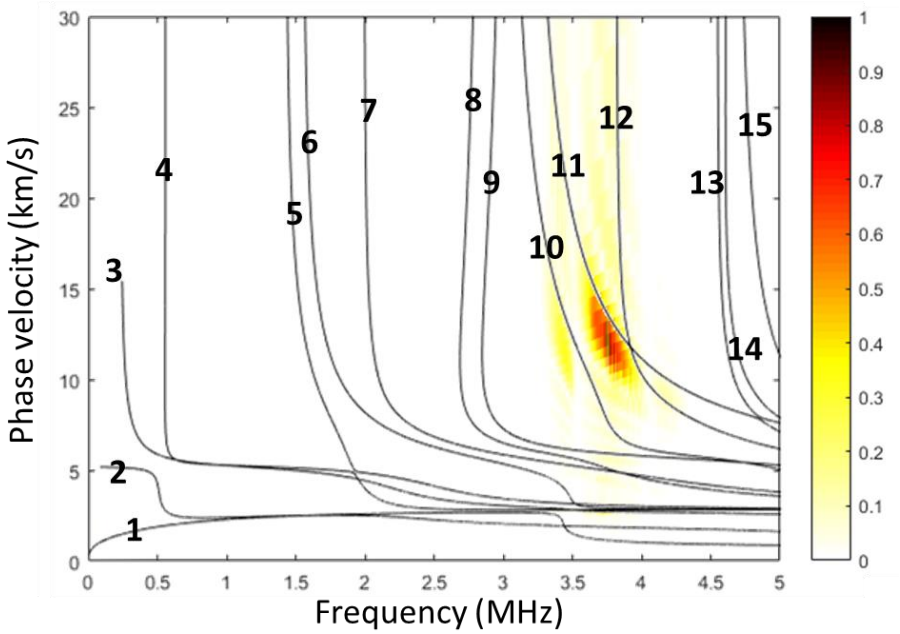

Figure 10 Frequency-phase velocity domain spectrogram of acquired out-of-plane displacements in the simulation model of bonded structure, overlapped with dispersion curve.

A comparison of out-of-plane displacement extracted from single point and superposed according to Eq. (3) is given in Figure 11. The signal from single point (see Figure 11a) shows that mode 11 is dominantly excited, but mingled with mode 10, mode 12, and reflected UGW. The superposed time domain signal (see Figure 11b) with a time delay corresponding to the skew angle 12.7^0 shows that mode 11 is the first-arrival wave and it is distinctly separated from modes 10 and 12 in the time domain. This phenomenon is attributable to that mode 11 between 3.5 MHz and 4 MHz has a larger group velocity than modes 10 and 12 (see Figure 3d), this enabling the separation and isolation of UGW mode 11 wave packet to be analyzed.

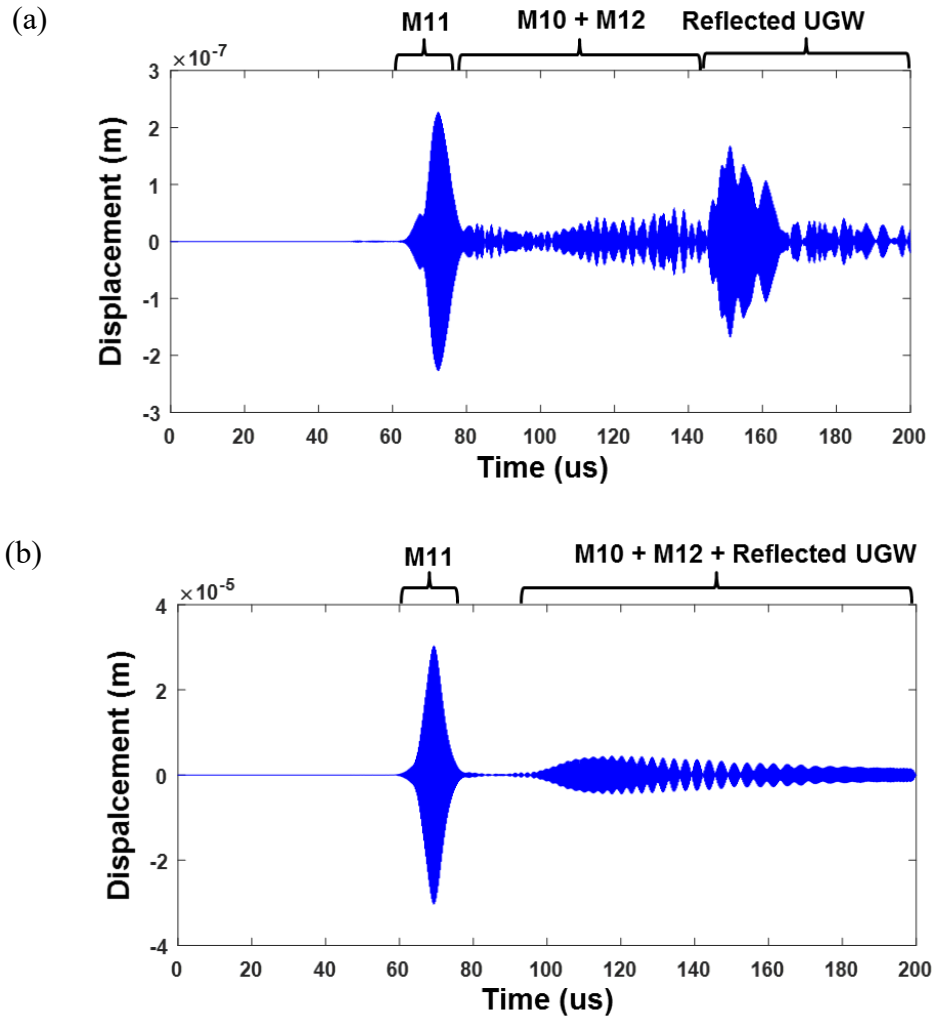

Figure 11 Simulated out-of-plane displacement (a) extracted from single point and (b) superposed according to Eq. (3).

Simulated and experimentally obtained wave packets for intact and disbonded structures are displayed in Figure 12a and b, respectively, which are well corroborated with each other, validating the correctness of the analysis. Note that the simulated signals in Figure 12a have been manually time-shifted to take the time delay of wave propagation in FABW into consideration, so as to be compared with experimental signals in Figure 12b. The signal amplitude of mode 11 drops monotonously with the increase of disbond size. Via the fast Fourier transform processing, the obtained energy spectrum of the superposed signals is observed to be dominantly distributed in the frequency range from 3.6 MHz to 4 MHz. Therefore, the normalized signal magnitudes from the theoretical analysis via SAFE-NME are

averaged on this range, and they are compared quantitatively with the normalized signal magnitudes from FEA and experiments as displayed in Figure 13, showing a good agreement. The experimental results always show a more drastic magnitude drop than results from theoretical analysis and the FEA. This discrepancy might be attributed to the wave scattering in the real three-dimensional experimental sample, which is not considered in the simplified two-dimensional theoretical analysis and FEA model. Based on the current results, the 10 mm disbond only corresponds to an amplitude drop of less than 20% compared with the intact bonded structure, which makes it barely identified, especially when there exist some noises. The other two disbond sizes, i.e. 20 mm and 40 mm, can be identified easily and evaluated quantitatively.

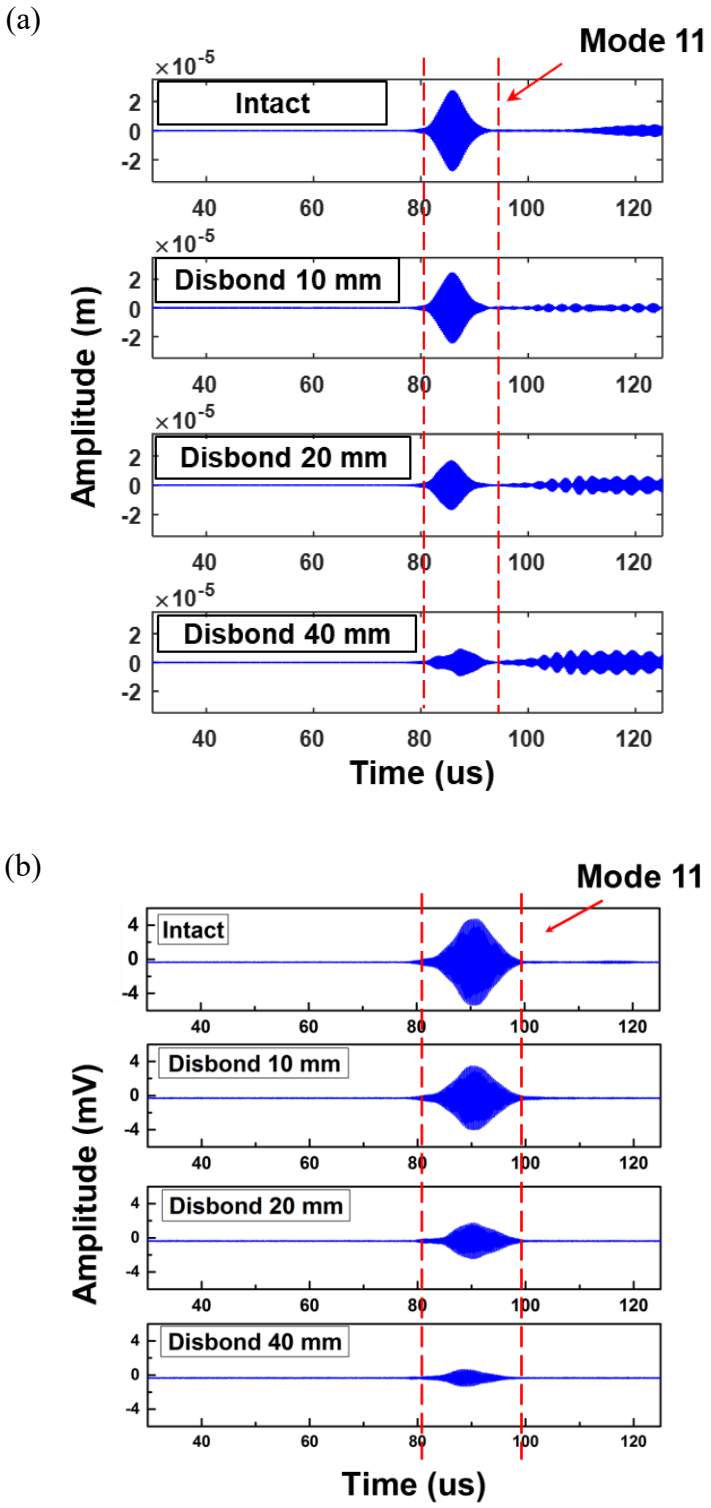

Figure 12 (a) Simulated and (b) experimental time domain signals in the cases of intact and disbond of 10 mm, 20 mm, and 40 mm.

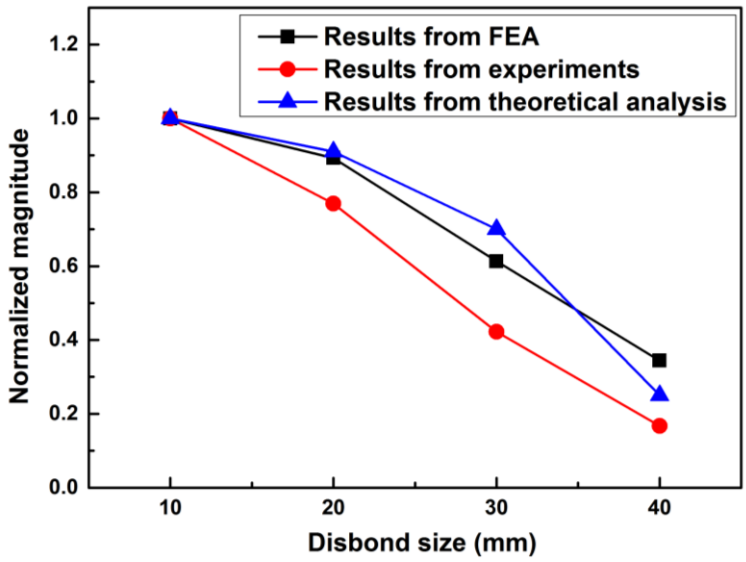

Figure 13 Comparison of signal amplitude obtained from theoretical SAFE-NME analysis, FEA, and experiment.

The signal magnitudes from the 50 scan paths are displayed in Figure 14. Signal magnitudes on most paths remain a value around 4.6 mV, a manifestation of 'no disbond', while a slight signal magnitude drop is observed on paths 6-8, which traverses the 10 mm disbond. This drop increases with the disbond size, as exhibited on paths 10-14 for the 20 mm disbond and paths 18-23 for the 40 mm disbond. In the extreme case, on the paths traversing all the three disbonds, i.e. path 37-42, the signal magnitude is marginal. Following this methodology, the disbond can be potentially identified and its size can be evaluated in a quantitative manner. In practical applications, the measurement of signal magnitude can be affected by factors including (1) multiple contact interfaces in the wave propagation process, and (2) external loading and temperature variation. These practical factors might influence the sensitivity of the selected UGW mode to disbond defect. Therefore, to enhance the accuracy of disbond evaluation, following approaches can be exploited and studied: (1) replacing FABW with fixed angle beam wedge; (2) gluing the interface between transducer and wedge; (3) developing some automatic gripping and loading apparatus to ensure a consistent coupling between wedge and experimental sample; and (4) investigating the influence of external environment on disbond

evaluation.

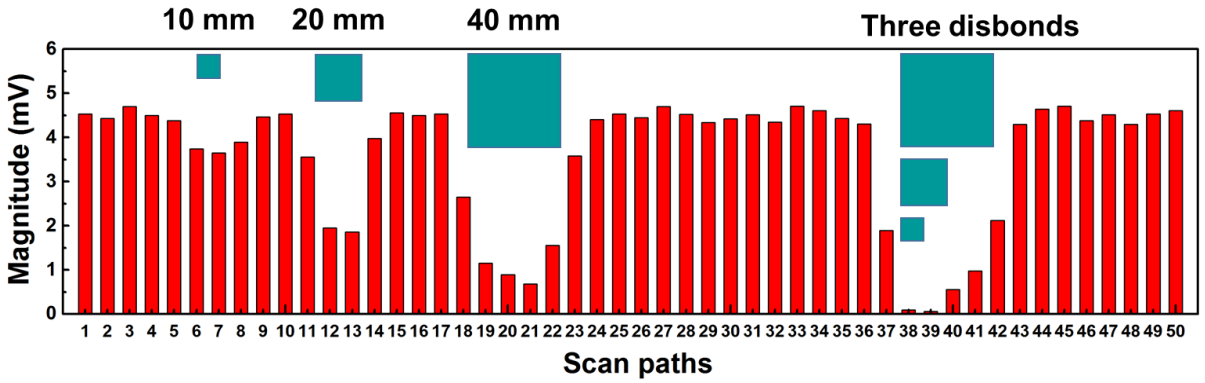

Figure 14 Magnitude of signals obtained from 50 scan paths.

4. Concluding remarks

Targeting detection and sizing of disbond in multilayer bonded structure, a dedicated framework is proposed and realized to make use of modally selective UGW, which is preferably excited and sensed with piezoelectric transducer mounted on angle beam wedges. In this framework, three key issues are addressed, including the UGW excitability/sensibility, the mechanism behind the interaction of UGW with disbond of different sizes, and separation of preferred UGW mode from other UGW modes. A detailed analytical derivation, numerical simulation, and experimental validation is performed in this study, whose results show that (1) for UGW at most mode frequency combination, disbond between adhesive and adherend layers is unable to largely reflect incident energy back, but fulfills a function of UGW mode conversion, enabling the possibility of disbond characterization; (2) the termed "true" UGW guided by adhesive layer (i.e., UGW mode with energy dominantly confined within the adhesive layer) suffers a poor excitability from surface loading. Finally, mode 11 at 3.85 MHz shows a monotonous magnitude drop upon traversing disbond of increasing sizes from 10 mm to 40 mm. Together with a large excitability and fast propagation velocity, these attributes make this selected UGW mode-frequency combination a good candidate for quantitative disbond detection and sizing.

Thus this line-to-line scanning method using modally selective UGWs enables highly improved efficiency of disbond detection and easy access to hidden regions, in comparison to the conventional point-to-point ultrasonic bulk wave-based method.

It is noteworthy that the optimal mode and frequency for different structures, which enables the disbond evaluation, is different, since the propagation property of UGW in the structure varies against the material properties. For example, for fiber reinforced plastic composite with resin as matrix, the proposed method shall take the dissipation of UGWs, which is related with the damping of resin, into consideration as well. Hence, considering the complexity of wave propagation in composite structures, the application of the proposed framework on detection and sizing of disbond for adhesive composite joint entails further investigation. Despite that, the framework proposed in this study provides a cornerstone for the selection of the candidate mode and frequency.

Acknowledgement

Menglong Liu and Fangsen Cui want to thank the Institute of High Performance Computing for the use of computational resources to carry out this research. Kai Wang wants to thank Composites & Fabrication Stream, Industrial Centre, The Hong Kong Polytechnic University for the preparation of experimental specimen. Zhongqing Su would like to acknowledge the support from the Hong Kong Research Grants Council via a General Research Fund (Nos.:15201416 and 15212417), and the support from the National Natural Science Foundation of China (No. 51635008).

References

1. Higgins A. Adhesive bonding of aircraft structures. *Int J Adhes Adhes* 2000; 20: 367–376.

2. Chester RJ, Walker KF, Chalkley PD. Adhesively bonded repairs to primary aircraft structure. *Int J Adhes Adhes* 1999; 19: 1–8.
3. Da Silva LFM, Adams RD. Joint strength predictions for adhesive joints to be used over a wide temperature range. *Int J Adhes Adhes* 2007; 27: 362–379.
4. Marques EAS, da Silva LFM. Joint strength optimization of adhesively bonded patches. *J Adhes* 2008; 84: 915–934.
5. Sohn H, Dutta D, Yang JY, et al. Automated detection of delamination and disbond from wavefield images obtained using a scanning laser vibrometer. *Smart Mater Struct* 2011; 20: 45017.
6. Park B, An YK, Sohn H. Visualization of hidden delamination and debonding in composites through noncontact laser ultrasonic scanning. *Compos Sci Technol* 2014; 100: 10–18.
7. Ciminello M, Concilio A, Galasso B, et al. Skin–stringer debonding detection using distributed dispersion index features. *Struct Heal Monit* 2018; 17: 1245–1254.
8. Johannes SP, Robin H, René F, et al. A sensor detecting kissing bonds in adhesively bonded joints using electric time domain reflectometry. *NDT E Int* 2018; 102: 114–119.
9. De Angelis G, Dati E, Bernabei M, et al. Development on aerospace composite structures investigation using thermography and shearography in comparison to traditional NDT methods. In: *2015 IEEE Metrology for Aerospace (MetroAeroSpace)*. 2015, pp. 49–55.
10. Zhang K, Zhou Z. Quantitative characterization of disbonds in multilayered bonded composites using laser ultrasonic guided waves. *NDT E Int* 2018; 97: 42–50.
11. Yashiro S, Wada J, Sakaida Y. A monitoring technique for disbond area in carbon fiber--reinforced polymer bonded joints using embedded fiber Bragg grating sensors: Development and experimental validation. *Struct Heal Monit* 2017; 16: 185–201.
12. Nondestructive Bond Testing for Aircraft Composites, https://www.olympus-ims.com/en/applications/non-destructive-bond-testing-aircraft-composites/ (accessed 11 March 2019).
13. Yuan S, Ren Y, Qiu L, et al. A multi-response-based wireless impact monitoring network for aircraft composite structures. *IEEE Trans Ind Electron* 2016; 63: 7712–7722.
14. Qiu L, Yuan S, Boller C. An adaptive guided wave-Gaussian mixture model for damage monitoring under time-varying conditions: Validation in a full-scale aircraft fatigue test. *Struct Heal Monit* 2017; 16: 501–517.
15. Qiu L, Yuan S, Zhang X, et al. A time reversal focusing based impact imaging method and its evaluation on complex composite structures. *Smart Mater Struct*; 20. Epub ahead of print 2011. DOI: 10.1088/0964-1726/20/10/105014.
16. Su Z, Ye L, Lu Y. Guided Lamb waves for identification of damage in composite structures: A review. *J Sound Vib* 2006; 295: 753–780.
17. Puthillath P, Rose JL. Ultrasonic guided wave inspection of a titanium repair patch bonded to an aluminum aircraft skin. *Int J Adhes Adhes* 2010; 30: 566–573.

18. Quaegebeur N, Micheau P, Masson P, et al. Methodology for optimal configuration in structural health monitoring of composite bonded joints. *Smart Mater Struct* 2012; 21: 105001.
19. Ong WH, Rajic N, Chiu WK, et al. Lamb wave--based detection of a controlled disbond in a lap joint. *Struct Heal Monit* 2018; 17: 668–683.
20. Cawley P, Pialucha T, Lowe M. A comparison of different methods for the detection of a weak adhesive/adhrend interface in bonded joints. *Rev Prog Quant Nondestruct Eval* 1993; 12: 1531–1538.
21. Fromme P, Reymondin J-P, Masserey B. High Frequency Guided Waves for Disbond Detection in Multi-Layered Structures. *Acta Acust united with Acust* 2017; 103: 932–940.
22. Ren B, Lissenden CJ. Modal content-based damage indicators for disbonds in adhesively bonded composite structures. *Struct Heal Monit* 2016; 15: 491–504.
23. Rokhlin SI. Lamb wave interaction with lap-shear adhesive joints: Theory and experiment. *J Acoust Soc Am* 1991; 89: 2758.
24. Lanza di Scalea F, Rizzo P, Marzani A, et al. Propagation of ultrasonic guided waves in lap-shear adhesive joints: case of incident A 0 Lamb wave. *J Acoust Soc Am* 2004; 115: 146–156.
25. Lowe MJS, Challis RE, Chan CW. The transmission of Lamb waves across adhesively bonded lap joints. *J Acoust Soc Am* 2000; 107: 1333–1345.
26. Song W, Rose JL, Galán JM, et al. Ultrasonic guided wave scattering in a plate overlap. *IEEE Trans Ultrason Ferroelectr Freq Control* 2005; 52: 892–903.
27. Miao H, Huan Q, Wang Q, et al. A new omnidirectional shear horizontal wave transducer using face-shear (d24) piezoelectric ring array. *Ultrasonics* 2017; 74: 167–173.
28. Liu M, Wang K, Lissenden CJ, et al. Characterizing hypervelocity impact (HVI)-induced pitting damage using active guided ultrasonic waves: From linear to nonlinear. *Materials (Basel)*; 10. Epub ahead of print 2017. DOI: 10.3390/ma10050547.
29. Kannajosyula H, Puthillath P, Lissenden CJ, et al. Interface waves for SHM of adhesively bonded joints. In: *7th International Workshop on Structural Health Monitoring: From System Integration to Autonomous Systems, IWSHM 2009*. 2009, pp. 247–254.
30. Giurgiutiu V. Tuned Lamb wave excitation and detection with piezoelectric wafer active sensors for structural health monitoring. *J Intell Mater Syst Struct* 2005; 16: 291–305.
31. Shen Z, Chen S, Zhang L, et al. Direct-write piezoelectric ultrasonic transducers for non-destructive testing of metal plates. *IEEE Sens J* 2017; 17: 3354–3361.
32. Predoi M V, Castaings M, Hosten B, et al. Wave propagation along transversely periodic structures. *J Acoust Soc Am* 2007; 121: 1935–1944.
33. Hayashi T, Song WJ, Rose JL. Guided wave dispersion curves for a bar with an arbitrary cross-section, a rod and rail example. *Ultrasonics* 2003; 41: 175–183.
34. Rose JL. *Ultrasonic guided waves in solid media*. Cambridge university press. Epub ahead of print 2014. DOI: 10.1017/CBO9781107273610.

35. Puthillath P. *Ultrasonic guided wave propagation across waveguide transitions applied to bonded joint inspection*. The Pennsylvania State University, 2010.